Optical Component Performance for the Ocean Radiometer for Carbon Assessment (ORCA).

Manuel A. Quijada, Mark Wilson, Eugene Waluschka, and Charles R. McClain

Goddard Space Flight Center, Greenbelt, MD 20771;

ABSTRACT

The Ocean Radiometer for Carbon Assessment (ORCA) is a new design for the next generation remote sensing of ocean biology and biogeochemistry. ORCA is configured to meet all the measurement requirements of the Decadal Survey Aerosol, Cloud, and Ecology (ACE), the Ocean Ecosystem (OES) radiometer and the Pre-ACE climate data continuity mission (PACE). Under the auspices of a 2007 grant from NASA Research Opportunity in Space and Earth Science (ROSES) and the Instrument Incubator Program (IIP) , a team at the Goddard Space Flight Center (GSFC) has been working on a functional prototype with flightlike fore and aft optics and scan mechanisms. As part of the development efforts to bring ORCA closer to a flight configuration and in order to reduce cost, we have conducted component-level optical testing using standard spectrophometers and system-level characterizations using nonflight commercial off-the-shelf (COTS) focal plane array detectors. Although these arrays would not be able to handle flight data rates, they are adequate for optical alignment and performance testing. The purpose of this presentation is to describe the results of this testing performed at GSFC and the National Institute of Standards and Technology (NIST) at the component and system level. Specifically, we show results for ORCA's spectral calibration ranging from the near UV, visible, and near-infrared spectral regions.

Keywords: ORCA, spectral calibration, polarization, ACE, OES, CO2 remote sensor

1. INTRODUCTION

The Ocean Radiometer for Carbon Assessment (ORCA) is a new design concept for a next generation ocean color remote sensing satellite. A major goal for this is similar as in previous earth remote sensing mission such as the Earth Observing System, including the Moderate Resolution Imaging Spectroradiometer[1] (MODIS), and others is to accurately measure Top-of-Atmosphere (TOA) and surface-leaving radiance $L_\omega(\lambda)$. In ocean-color remote sensing, the sensor-measured radiance at the top of the ocean atmosphere system, measured at wavelength λ, can be written as[2]

$$L_t(\lambda) = L_r(\lambda) + L_a(\lambda) + L_{ra}(\lambda) + t(\lambda)L_{\omega c} + t(\lambda)L_\omega, \quad (1)$$

where $L_r(\lambda)$, $L_a(\lambda)$, and $L_{ra}(\lambda)$ are contributions, respectively, from the multiple scattering of air molecules Rayleigh scattering with no aerosols, aerosols no air molecules, and Rayleighaerosol interactions. The $L_{\omega c}(\lambda)$ is the radiance at the sea surface that arises from sunlight and skylight reflecting from whitecaps on the surface. The $L_\omega(\lambda)$ is the water-leaving radiance that is the desired quantity in ocean-color remote sensing to relate the ocean near surface physical and bio-optical properties and $t(\omega$ is the atmospheric diffuse transmittance that accounts for the effects of propagating L_ω and $L_{\omega c}$ from the sea surface to the TOA. In particular, this atmospheric correction is the main challenge in converting measured TOA radiance L_r to L_ω.

Further author information: (Send correspondence to M.A.Q.)
M.A.Q.: E-mail: manuel.a.quijada@nasa.gov, Telephone: 1 301 286 3544

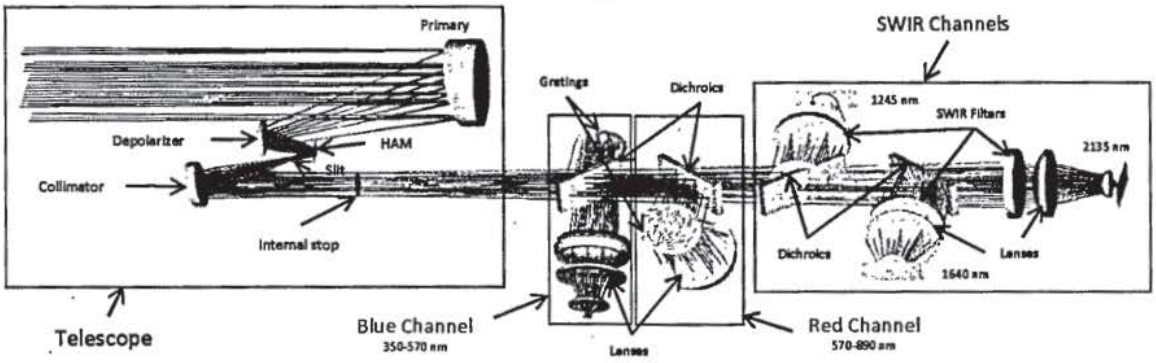

Figure 1. Diagram showing Collimator mirror and ORCA front-end optics.

2. ORCA OPTICAL SYSTEM

The development of the design and testing of a ORCA prototype has been under way at the Goddard Space Flight Center (GSFC) since 2007. This work has been supported under the auspices of a NASA Research of Opportunity in Space and Earth Science (ROSES) and the Instrument Incubator Program (IIP). ORCA is envisioned as a possible successor to the SeaWif instrument.[3] The instrument design reflects lessons learned from heritage sensors and is tailored to the new observational requirements recognized for advancing research in ocean biology and biogeochemistry. A second paper in these proceedings will present a more detailed optical design.[4] The design requirements include a high spectral resolution (5nm) from UV through visible and short-wave infrared (SWIR) wavelengths (350-2140 nm). There will be a minimum of 26 aggregate bands with a total signal-to-noise (SNR) to exceed 1500 in most UV and visible aggregate bands. There will be a 2-day global coverage at approx. 1.0 Km resolution (noon/sun-synchronous orbit required). Other requirements are:

- Minimal sun glint contamination (sensor tilt required)
- Minimum polarization sensitivity (polarization scrambler required)
- Minimum and well characterized out-of-band response, electronic cross-talk, and stray light
- Minimal image striping
- No band saturation over bright targets
- Solar and lunar on-orbit calibration (spacecraft pitch maneuver or 90 tilt required)
- Complete sensor optical model and flight-like EDU

The observational requirements listed above reflect our new understanding of marine systems and their influence on ocean optics. Therefore, these requirements will not be met by any simple expansion of the SeaWiFS or MODIS designs. It is for this reason that these requirements have driven the optical design to include a grating spectrometer. Using diffractive gratings seems an obvious choice in order to simplify the optical design. However, this represents a challenge for a instrument with a polarization sensitivity requirement of less than 1%, given that gratings themselves tend to produce a substantially polarized output beam (as a high as 40%). The proposed solution has been, like in SeaWifs, to incorporate a depolarizer in order to produce a polarization insensitive optical design. Another paper to be published in these proceedings will described in greater details the design and characterization of such depolarizer.[5]

Figure 1 has a layout of the ORCA optical system. The front-end part includes a telescope system with a primary mirror, depolarizer, half-angle mirror (HAM) and slit. After the slit there is a collimator mirror followed by the spectrograph area that is divided in three main sections: a blue channel with spectral coverage from 350

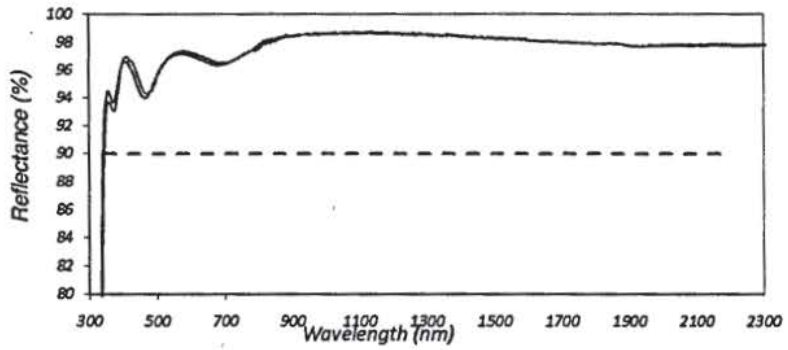

Figure 2. Typical Optical reflectance for ORCA pirmary, HAM, and collimator mirrors.

to 570 nm, a red channel that includes a wavelength range from 570 to 890nm, and a Short Wave Infrared (SWIR) channel with three discreet bands at 1245, 1640, and 2135 nm. Next sections will describe in more details characterizations for the telescope optical elements as well as the optical components that form part of ORCA three main channels.

2.1 Telescope Optical Components

The ORCA front-end optical system (a schematic of which is shown on the left side of Fig. 1) consists of a telescope with a primary mirror that collects collimated light from an object at infinity and images it onto a slit. But before the light reaches the slit, it is intercepted by a polarization scrambler with a reflective coating on the back side, and a double sided half-angle mirror (HAM), that folds the light on the slit as shown in Fig. 1. As mentioned earlier, the purpose of this polarization scrambler is to reduce the polarization sensitivity of the ORCA telescope. It is placed right after the primary mirror in order to prevent any polarization for the scene under observation to propagate through the rest of the spectrograph. The scanning mechanism is such that both primary mirror and HAM will rotate in synchronization mode around same axis with HAM rotating at half the speed as that of the primary.

2.2 Primary Mirror

The Primary Mirror (PM) of ORCA is a a off-axis ellipsoid (OAE) focusing mirror with a 90 mm clear aperture (100 mm physical diameter), whose optical prescription is as follows. This mirror has vertex radius of 600 mm with a focal length ($F1$) of 304 mm and off-axis focusing distance of 50 mm. The surface figure error was specified to $\lambda/20$ RMS. We performed micro roughness using a ADE Phase-Shift (MicroXAM model) surface profiler and we found the RMS roughness is ~ 10 $\AA$. We will discuss next the performance of the reflecting coating applied to the primary as well as the reflecting components such as the HAM, depolarizers and the collimator mirrors.

2.3 UV-Enhanced Ag Coating

Figure 2 illustrate the performance of the coating used on the primary as well as the HAM mirrors. It is a proprietary version of UV-enhanced protected Ag coatings. The reflectance where measured using a Perking-Elmer 950 spectrophotometer fitted with a Universal Reflectance Accessory (URA) that provides absolute reflectance as function of wavelength (200-3300nm) and Angle of Incidence (AOI) from 8° to 68°. The reflectance data in Fig. 2, taken at the nominal AOI of 15°, indicate this is a high-throughput coating with an average reflectance of $\sim 98\%$ in the 350 to 2200 nm range. These data also display interference oscillations below 800nm that are most likely caused by the dielectric overcoats that most likely are used to protect the Ag metal underneath and also to boost the reflectance around the natural roll-off of Ag that occurs below 400 nm. The 4% reflectance enhancement realized with this coating between 350-400 nm (when compared to bare Ag) provided the deciding factor in choosing this coating for ORCA. This was required in order to meet the SNR requirement at the shortest blue-channel band centered at 350 nm. We also investigated the polarization properties for this coating

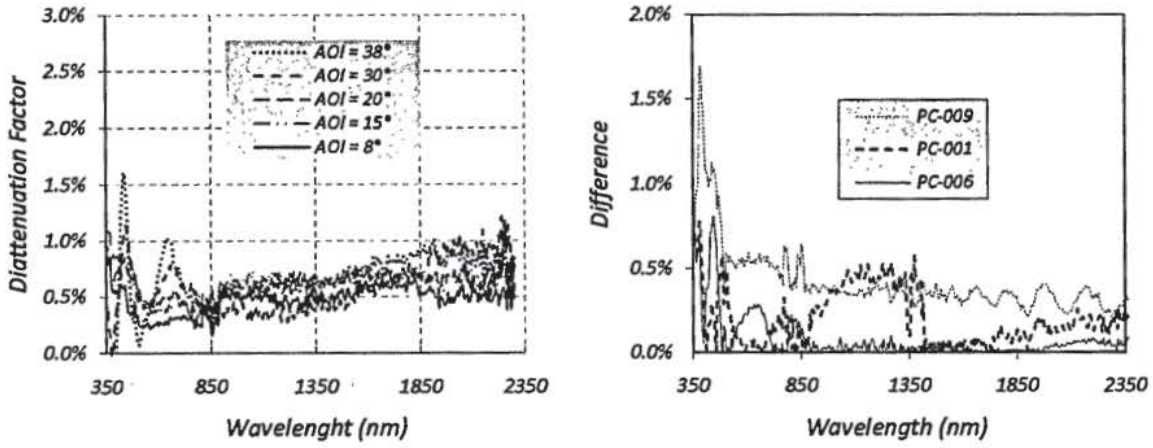

Figure 3. Polarization sensitivity data of UV-enhanced Ag coating obtianed from measured R_s and R_p.

by measuring reflectance for R_s and R_p polarized light at various AOI from near-normal (8°) to about 38°. We then calculated a diattenuation factor (DF) that is defined by:

$$DF = \frac{(R_s - R_p)}{R_s + R_p}. \tag{2}$$

The results of these calculations are shown on the left side of Fig. 3. These results suggest a UV-enhanced Ag coating with a fairly low polarization sensitivity, with the average DF value below 1% for most of the range shown. Only for AOI equal to or larger than 38° we observe that DF slightly exceeds the 1% threshold specially at wavelengths shorter than 500nm.

Another consideration is how much variability there is in the coating process from one run to the next. This is very important given that the HAM optics will have both sides coated with the same reflecting coat. Hence in scanning mode, ORCA will be using one side of the mirror half the time, and the other side will be used the other half. The use given to this mirror imposes a very tight requirement from the instrument calibration point of view in that differences in reflectance from one side to the other would be kept to a minimum. The right panel in Fig. 3 shows the calculate reflectance difference from side 1 and side 2 of three HAM's that were coated. The results show a difference in response from either side that varies from sample to sample. The sample labeled "PC-006" offers the smallest ($\simeq 0.09\%$) average difference of the three, and for this reason this was HAM chosen to install on the instrument. Even though small differences could in principle be calibrated out, it is very reassuring how small the differences were (for mirror "PC-006" in particular) in the coating process used to produce this version of UV-enhanced protected Ag.

2.4 Depolarizer

The depolarizer is a commercially available scrambler made by Karl Lambrecht. It is made using the principle of the Cornu depolarizer consisting of two matching wedged pieces of magnesium fluoride crystals that are glued together so that the optics axis of one is rotated 45° with respect to the other piece.[6] Any ray entering this optics effectively passes through these two wave plates. The thickness of these and therefore their retardance varies across the beam. For this reason, they are considered area depolarizer, since at different ray heights on the entrance face of the cube, different thicknesses of left-and-right-hand crystal are traversed resulting in an exit polarization angle that is a function of ray height. Thus, the beam will have its polarization state mixed over the beam face. It is also worth mentioning that the phase shift, and hence polarization state mixing are also dependent on wavelength due to dispersion in the glass. The manufacturer of this optic suggests using it in transmission mode where polarized light enters on one side and it emerges unpolarized on the other. However this is not the way in which it will be in the ORCA optical system. As the left panel of Fig. 4 shows, we have

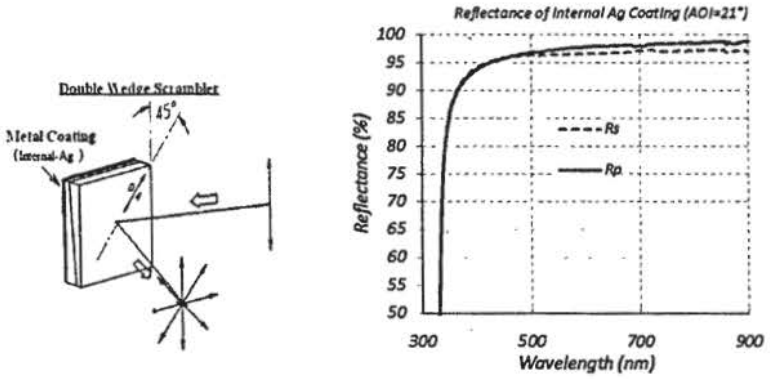

Figure 4. Left panel: Polarization scrambler used in reflectance mode made with two wedge pieces of magnesium fluoride. Right panel: Measured polarized reflectance on scrambler at a AOI =21°.

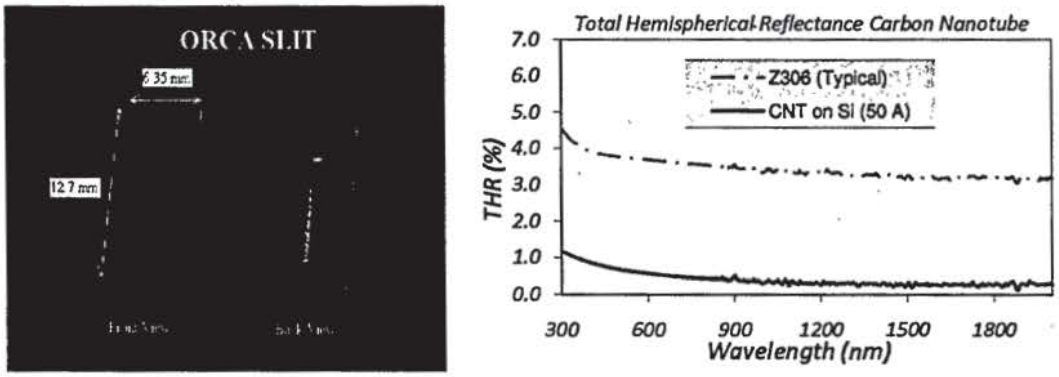

Figure 5. Left panel: Front and back slit image with external dimensions. Right panel: Spectral performance of Z306 and carbon nanotube black coatings on Si substrate.

coated one side of the optics with a reflective coating of protected internal Ag. Hence, the optics is used in a reflection mode (as shown on the left panel of Fig. 4), where the depolarizing effect occurs as the beam enters through the non-coated side, goes through the two segmented wedges, then it gets reflected on the coated back and emerges on the same side with a AOI $\simeq$21°. This is called a double-pass configuration and it is similar to what was done in the SeaWiFS instrument.[3]

The right side of Fig. 4 display the measured reflectance of the scrambler coated on the back side with a proprietary internal Ag. The AOI was set in the same configuration as the optic will be used at the nominal value of 21°. The results in this figure show that the average reflectance is around 97%. Although this value is lower than bare Ag over the same wavelength range, it is consistent with the expected losses as light travels through the MgF2 glass.

2.5 Slit

The right side of Fig. 5 shows an image the slit used in ORCA. The front and rear surfaces are flat, while the opening in the rear side is beveled at 45° on each side to remove the possibility of vignetting as the light goes through it. It is made out of silicon substrate and its main function is to define the instrument field of view (IFOV) at the detector focal plane location. The dimensions of the clear opening are determined through a ray-tracing optical model to ensure that ORCA meets is stated optical performance requirements. For instance the long dimension ($\sim$ 8.0 mm) is in the along-scan (or spatial) direction and it is related to the instrument

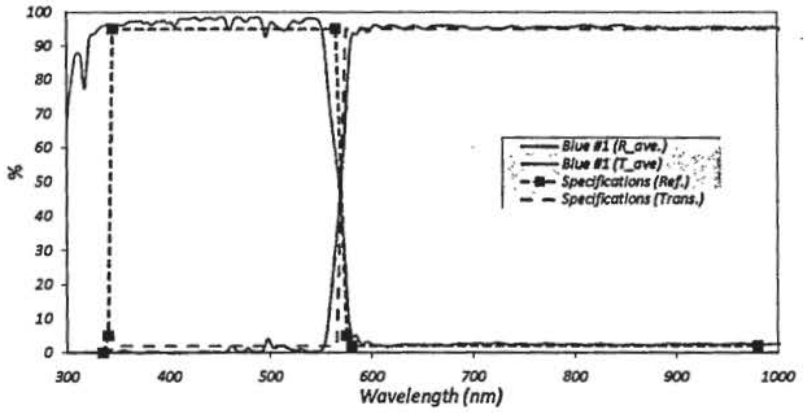

Figure 6. Average reflectance and transmittance curves for the blue-channel dichroics. The dashed line represents the specification given to the vendor prior to fabrication.

requirement of being able to resolve 1.0 Km targets on the ground. Similarly, the narrow ($\sim$ 0.65 mm) is along the across-scan (or spectral) direction and it sets the maximum spectral resolution.

Given the fact that the slit is located at the telescope best focus, it is required that light that bounces off does not become a source of scattered light that may contaminate the signal that goes through. The solution is to have an absorbing coating on the slit to reduce this possible source of stray light. To this end, we considered two alternatives: one was a conventional Z306 black pain that has a long heritage in spaceflight application. The second one was a Multi Walled Carbon Nanotube (MWCNT) coating that have been shown to represent the blackest materials known in nature.[7] To further evaluate the suitability of either of the two, the right panel of Fig. 5 shows total hemispherical reflectance (THR) measured on representative coatings for each of the two. These results show that indeed, the MWCNT coating has an almost factor of 10 better performance in terms of its ability to absorb light over the wavelength range shown in the figure. These results were a deciding factor in choosing the MWCNT on the ORCA slit that was eventually installed in the instrument. Another deciding factor was the fact that silicon is the ideal substrate on which to grow the MWCNT.

3. SPECTRAL RESPONSE

We now turn our attention at spectral characterization of the optical components in ORCA three main channels. The diagram in Fig. 1 show the arrangement of these with the blue channel being the first after the collimating mirror. The blue spectrograph is followed by the red channel and the three Short Wave Infrared single channels at the back end of the instrument. The following sections are organized according to the sequence in which these optical components appear in the instrument's optical train. Hence, we will discuss first the optical response of the dichroic beamsplitters.

3.1 Dichroics

The current design of the ORCA radiometer uses four dichroics. In the ORCA application, these dichroics transmits light for wavelengths above a reference wavelength in the dichroics design and reflect light below the reference wavelength. These dichroics perform a pre-filtering of the radiance from the earth, limiting the range of wavelengths that reach the next optics in each of the five focal planes.

The dichroics and focal plane assemblies in ORCA are shown in schematic form in Fig. 1. In the schematic, the first or blue-channel dichroic, which is set at AOI of 45°, reflects light in the 350-570 nm range onto the next optics in this channel. This dichoric is designed to transmit light in the 570-2200 nm. This light bundle is next intercepted by a second red-channel dichroic. This second dichroic set at a AOI of 45°, performs a second splitting of the light, reflecting wavelengths in the 580-890 nm range and transmitting radiance in the 900-2200

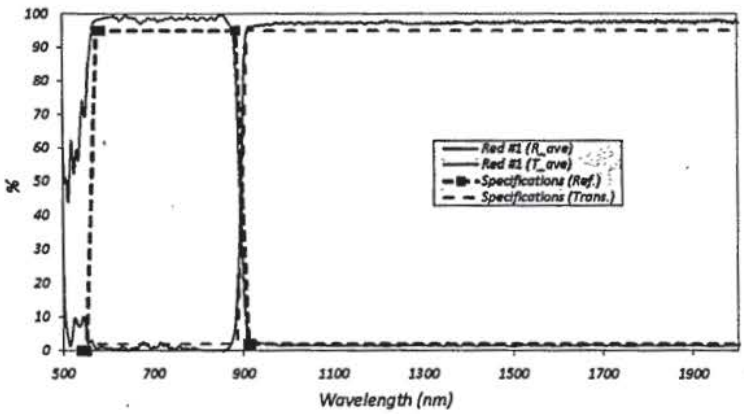

Figure 7. Average reflectance and transmittance curves for the red-channel dichroics. The dashed line represents the specification given to the vendor prior to fabrication.

nm range. Two more dichroics in the SWIR channel perform more pre-filtering for the three remaining bands in this channel. The SWIR dichroic 1 reflects energy in the 1230 to 1255 nm range. The transmitted light bundle is next splitted by a second SWIR dichroic 2 by reflecting radiance in 1600-1650 nm and transmitting light above 1700 nm on to the last SWIR band centered at 2135 nm.

Figure 6 gives the spectral response in the form of the average reflectance and transmittance for the ORCA blue-channel dichroic as a function wavelength. This figure show the in-band average reflectance and transmittance are >97% both cases indicating an excellent performance in this regard, when compared to specifications. However, the cut-off for the last 90% reflection point for this dichroic falls at 554.9 nm. This should be compared with the specification that the 90% wavelength be at 568 nm. It is evident that the vendor, missed the specified cut-off by about 13 nm. This is significant since the last band in the blue channel is centered at 555 nm (with a bandwidth of 15 nm). This caused the instrument to miss the 1% polarization requirement for this band only, given that it falls in the dichroic transition region (550 to 570 nm, where this optic produces a strongly polarized (*sim*100$) output. We should point out that moving the design cut-off upward by at least 15 nm will resolve this non-compliance polarization issue for this particular band. However, this may also require a tightening of the transition width range to minimize any loss in throughput from the adjacent red-channel band.

Figure 7 gives the average reflectance and transmittance for the ORCA red-channel dichroic as a function wavelength. We find that the in-band average reflectance and transmittance are 98% in both cases indicating an excellent performance in this regard. Also, the cut-off for the last 90% reflection point for this dichroic falls at 883.5 nm. This is in excellent agreement with the requirement of 885.0 nm.

Table 1. List of dichroics along with their corresponding center wavelengths and bandwidth parameters.

Dichroic Name	λ_0 (nm)	R_{ave} (%)	FWHM (nm)	λ_{cut-on} (50%) (nm)	$\lambda_{cut-off}$ (50%) (nm)	λ_{cut-on} (1%) (nm)	$\lambda_{cut-off}$ (1%) (nm)
Blue	437.7	96.8	234.2	< 300	568.4	N/A	577.1
Red	721.8	98.3	323.3	< 536	892.7	N/A	904.7
SWIR #1	1200.5	98.0	140.8	< 1101	1307.4	N/A	1332.9
SWIR #2	1632.0	94.9	165.9	< 1555	1721.1	1564.4	1749.8

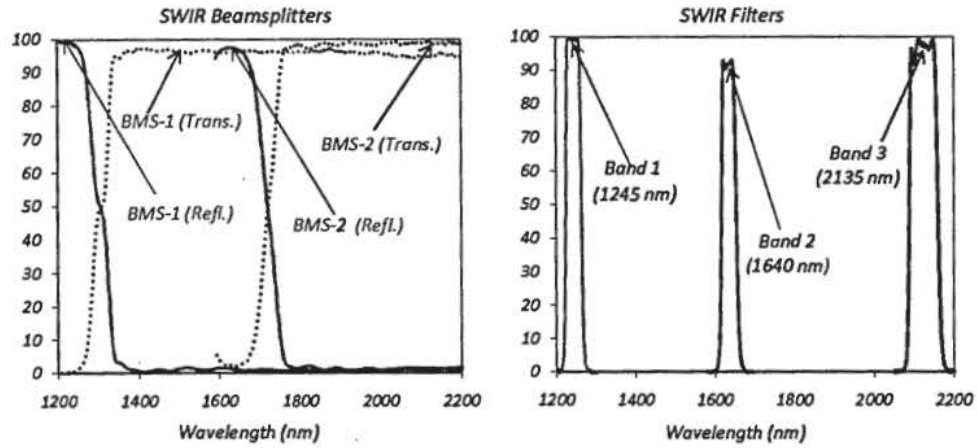

Figure 8. Left panel: Reflectance and transmittance for SWIR beamsplitters 1 and 2. Right panel: Transmittance for the band-pass filters for the three SWIR bands.

3.2 SWIR Optics

The left panel of Fig. 8 gives the average reflectance and transmittance for the two dichroics beamsplitters in SWIR channels. These spectra were collected at the operating angle of incidence of 45°. The first one labeled "BMS-1" splits the beam of light into a reflected component (1130-1270 nm) and a transmitted one (1270-2200 nm). The second dichroic (BMS-2) intercepts the transmitted component from BMS-1 and performs a second split into a reflected (1575-1690 nm) component and a transmitted one (1690-2200). The right side of Fig. 8 displays the transmission shape for each of the three SWIR dichroic filters. These are the optics that define the actual bandpass for each of the three SWIR bands at 1245, 1640, and 2135 nm. They are placed in front of the respective lenses that re-image the collimated beam on the back on the corresponding focal plane detectors. The filter responses give the principal definition of the SWIR bands in terms of: throughput from the average transmission , the center wavelength; the band edges from the full-width-half-maximum, and the extended band edges from the 1% points. Tables 1 and 2 give a summary for all the dichroic and filter parameters derived from

Table 2. List of narrow band-pass filters, along with their corresponding center wavelengths and bandwidth parameters.

Filter #	λ_0 (nm)	T_{ave} (%)	FWHM (nm)	λ_{cut-on} (50%) (nm)	$\lambda_{cut-off}$ (50%) (nm)	λ_{cut-on} (1%) (nm)	$\lambda_{cut-off}$ (1%) (nm)
Filter 1	1242.2	98.7	39.9	1222.5	1262.4	1218.0	1267.4
Filter 2	1634.0	91.1	38.0	1616.4	1654.4	1611.7	1661.3
Filter 3	2134.0	96.6	72.0	2089.3	2161.2	2084.0	2169.0

data shown in Figures 6, 7 and 8. Overall we observe these optics show good to excellent performance that will enable ORCA to meets its stated optical performance requirements.

3.3 Gratings

As discussed previously in Sec. 2, the hyperspectral nature of ORCA along with its high spectral resolution requirements have driven the design to include gratings to provide proper dispersion of the light. This seems an obvious choice given that diffraction gratings are optical components used to spatially separate polychromatic light (white light) into its constituent optical wavelengths. The simple grating consists of glass substrate with a series of parallel, equally spaced lines on the front surface of the glass. Diffraction gratings are used in such diverse fields as spectroscopy, colorimetry, metrology and laser optics. The next question is to determine the grating parameters, from an optical design model perspective, in order to meet the specifics application needs.

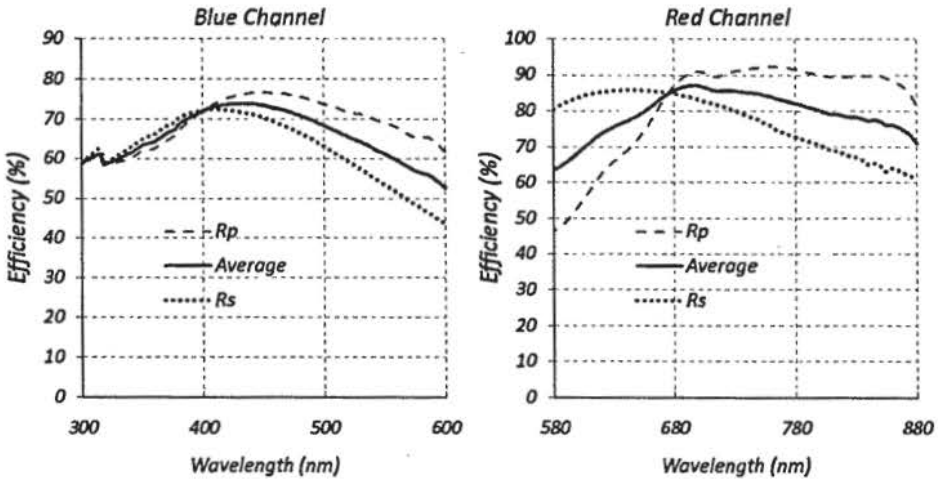

Figure 9. Left panel: Reflectance and transmittance for SWIR beamsplitters 1 and 2. Right panel: Transmittance for the band-pass filters for the three SWIR bands.

In the case of ORCA, its spectral resolution requirement is such that it will require projection of a monochromatic beam of light to cover an area on the focal plane of roughly 5nm/superpixel, where one superpixel is equal to 8 physical pixels with dimensions of 26×26 μm.[4] Hence, it follows that the grating parameters can be determined from the grating equation:

$$d(\sin\alpha \pm \sin\beta) = m\lambda, \tag{3}$$

where, α is angle of incidence, β is the angle of diffraction, d is the distance between adjacent grooves, m is the order (integer number) and λ is the wavelength of the incident beam. It is clear from Eq. 3 that the condition for the formation of a diffracted order depends on the wavelength, λ, of the incident light. Hence, to consider the formation of a spectrum we need to know how the angle of diffraction varies with the incident wavelength. This is found by differentiating Eq. 3 with respect to β, assuming the angle of incidence is constant:

$$\frac{d\beta}{d\lambda} = \frac{m}{d\cos\beta.} \tag{4}$$

The quantity $d\beta/d\lambda$, also known as the angular dispersion, is the change of diffraction angle corresponding to a small change of wavelength. Finally, the linear dispersion of a grating is the product of this term and the effective focal length of the optical system.

Another consideration to take into account in the case of ORCA is the physical size of the slit along the spectral direction (the narrow dimension of the slit image shown in Fig. 2.5). The specifics of how the equations above were used to determine the grating parameters for the ORCA instrument are discussed elsewhere.[4]

In addition to the dispersion requirements given above, the gratings were required to be flat and that conventionally ruled gratings will provide the minimum required average efficiencies across each of the ORCA blue and red channels. Finally, the gratings were used in such a way that there was not much difference between angle of incidence and the angle of the proper diffracted order ($\alpha \sim \beta$). This is was done to avoid anamorphic magnification of the slit image at the instrument focal plane. Figure 9 has the measured efficiencies for the two gratings used on the ORCA instrument. The left panel of this figure gives the data for the blue channel in the 300-600 nm range, whereas the right panel shows results for the red grating over the 580-880 nm range. Polarized and average efficiencies are plotted as a function of wavelength and these were measured at the appropriate AOI for either grating (28° for the blue and 35° for the red channels). We notice the measured efficiencies are at 60% or higher for both gratings. The polarization sensitivities are <10% for the blue grating, while it is <30% for the red one. A summary of these results are in shown in Table 3 where we also show the groove density for these gratings as well.

Table 3. Grating parameters for ORCA blue and red channels.

Channel	Groove Dens.	Order	AOI	Efficiency	Pol. Sen.
Blue	818 lines/mm	1st	28°	> 60%	< 18%
Red	703 lines/mm	1st	35°	> 60%	< 30%

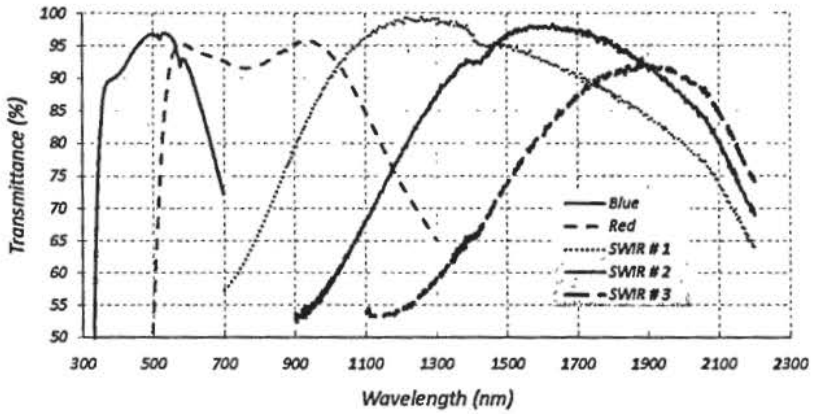

Figure 10. Total throughput for each lens assembly in ORCA five channels.

3.4 Lenses

The last optical element before the detector at each of ORCA five channels is a lens assembly. Each of the lenses picks up the collimated (and dispersed output of the gratings in the blue and red channels) and form an image of the light going through the slit on the back of the assembly at best focus where the CCD detectors will be located. The imaging performance requirements are such that these lenses would correct for known aberrations of ORCA (OAE) primary, while producing focused spots at the edges of the slit image (both spectral and spatial) of 1 physical pixel diameter, with a minimum of slit curvature. The blue-channel lens elements were constructed out of I-line glass materials, whereas standard Schott glass was the material of choice for the red-channel lens elements. The design requirements for both of those two lenses were fully met with all spherical surfaces. The elements in all three SWIR channels were made out of LAK9G15 glass. The throughput in each of the five lenses was maximized by the application of anti-reflection (A/R) coatings to reduce reflection losses. Those A/R coatings were tune to match the respective band-pass for each of the channels. Figure 10 display the throughput performance in each of the five lenses from measured transmittance as function of wavelength over the full ORCA bandpass range. These results show the A/R coating application was successful in maximizing the transmission in each of channel in-band spectral range. We find that for the blue band, the average in-band transmission is ~93.5%. Likewise, the red-channel transmission is ~ 93.1%. Finally, the corresponding transmission values for the SWIR are 98.9%, 97.7%, and 81.2% for channels 1 through 3 respectively.

4. SYSTEM-LEVEL PERFORMANCE

We are now in a position to calculate the total system-level throughput from the piece-part data we have shown in previous sections. These results will be of great importance when evaluating ORCA radiometric calibration and performance, as these results will form the basis to conclude whether ORCA will meet its stated radiometric science goals.

4.1 Throughput

The left panel of Fig. 11 illustrates the total efficiency response form the blue and red channels of ORCA. These curves are derived by multiplying through the average spectral response of each of the components in the ORCA optical train, including the grating efficiencies. An analysis of these results when compared to typical

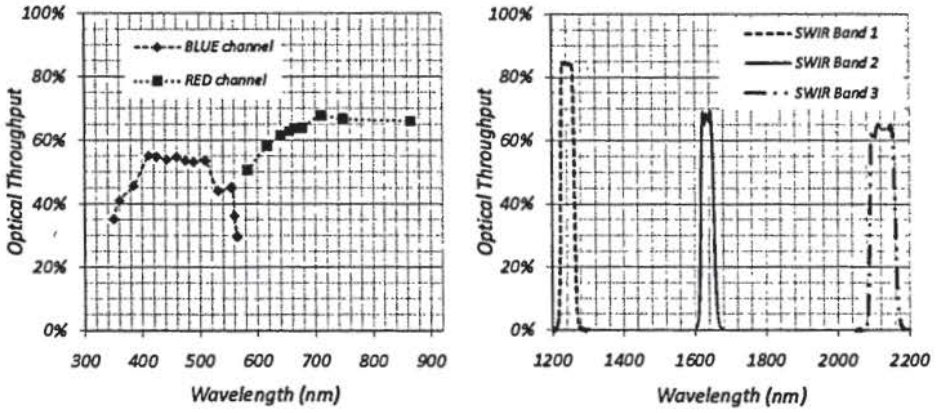

Figure 11. Total throughput for ORCA radiometer calculated from piece-part component data for blue and red channels (left) and three SWIR bands (right).

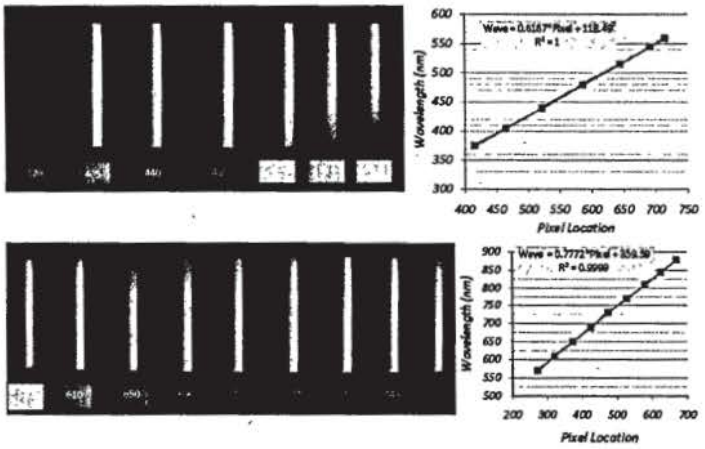

Figure 12. Left panel: Collection of slit images at variuos laser wavelengths for ORCA blue (top) and red (bottom) channels. Right panel: Linear plot of wavelength *vs* pixel location fro the corresponding images on the left.

surface-leaving radiance indicate that ORCA will meet or exceed the radiometric performance of either MODIS or SeaWif. These calculations show that ORCA should have not problem in meeting its sensitivity requirement goals in order to deliver ocean-color data product over the 20 aggregated bands in the 350-885 nm wavelength range. The overcall efficiency is decidedly lower in the blue channel, when compared to the red-channel results. However, we should point out that measuring surface-leaving radiance in the red-channel spectral range will be more challenging given that signals there are much weaker. Hence, the higher sensitivity from these piece-part data would compensate for these weaker signals in the red band. The right panel Fig. 11 shows similar calculations done for the three bands in the SWIR channel. We should notice that these curves provide information about the total throughput as well as the spectral bandwidth for each of those bands. This is on account that narrow-band filters are used to define the transmission band-pass in each of the three SWIR channels. We will discuss next dispersion information about the blue and channels.

4.2 Dispersion

As mentioned previously, the ORCA optical design incorporates gratings in the blue and red channels to provide the proper wavelength sorting. Because of how gratings are implemented in this design, it is not possible to get the

overall system dispersion characteristics by just looking at the grating dispersion properties alone. The approach we followed was to perform system-level characterization using non-flight commercial off-the-shelf (COTS) focal plane array detectors. The format for these arrays is 256×1032 with individual pixel size of 26 × 26 μm. They are placed at best focus behind the respective blue- and red-channel lens assemblies. Although these arrays are oversized and they would not be able to handle flight data rates, they are adequate for optical alignment and performance testing. The testing configuration consisted of placing ORCA in front of an integrating sphere that was coupled to a tunable laser that allowed the instrument to be illuminated with monochromatic light of known wavelength. The sphere had an aperture larger than that of ORCA in order to have the slit uniformly illuminated. A series of images were recorded at varying laser wavelengths. Performing these tests required relocating the instrument to one of the radiometric laboratories at the National Institute of Standards and Technology (NIST).

The left panels of Figure 12 show results of a series of images taken at various laser wavelengths in the corresponding spectral range for the blue (top) and red (bottom) channels of ORCA. These figures show projections of the slit images on the CCD arrays of either channel. The horizontal dimension corresponds to the spectral direction, whereas the vertical direction is the spatial direction. The extend and separations of the slit images provide information about the instrument dispersion properties. For instance, the full-width-half-maximum along the spectral direction for the slit images shown in Fig. 12 are ~ 6 and ~ 7 pixels for the blue and red channels respectively. The extend along the vertical (spatial) direction is roughly 135 pixels. Determination of the centroid for each of these to find their location on the CCD arrays and plotting these pixel locations *vs* their corresponding wavelengths allowed us to estimate the overall instrument dispersion and wavelength calibration performance. The right panels of Fig. 12 show the results of these analysis. In the case of the blue channel, the slope yields a value of 0.62 nm/pixel while this number is 0.78 nm/pixel for the red band. Given that a superpixel in ORCA consists of 8 physical pixels, we find the overall dispersion is roughly 4.96 nm/superpixel for the blue and 6.2 nm/superpixel for the red channel. A comparison of these numbers with predictions from the optical design models suggest that these numbers are right on target for blue channel, while only slightly higher for the red-channel dispersion requirement.

5. CONCLUSIONS

In conclusion, the results obtained from component-level optical testing have validated the robustness of the optical system design for ORCA. All the optical components used in the ORCA prototype have been made using existing technology and their excellent performance have brought ORCA closer to a flight configuration. The predicted optical throughput from piece-part data, the system-level dispersion measurement and polarization sensitivity results have shown ORCA is in a position to meet or exceed the radiometric requirements of the Decadal Survey Aerosol, Cloud, and Ecology (ACE), the Ocean Ecosystem (OES) radiometer and the Pre-ACE climate data continuity mission (PACE).

ACKNOWLEDGMENTS

We would like to acknowledge Steve Brown, Ping-Shine Shaw, and Keith Lykke (National Institute of Standards, Gaithersburg, MD) for their invaluable assistance during ORCA optical testing activities at NIST. We would like to acknowledge Alan Holmes (SBIG, Inc., Santa Barbara, CA) for his insight in the radiometric calibration techniques used on SeaWif and their application to ORCA. Finally, we would also like to thank Tim Madison from the Optics Branch (NASA-GSFC, Greenbelt, MD) for his help during the integration and alignment phase of the ORCA prototype.

REFERENCES

1. Gerhard Meister, Ewa J. Kwiatkowska, Bryan A. Franz, Frederick S. Patt, G. C. Feldman and C. R. McClain, "Moderate-resolution imaging spectroradiometer ocean color polarization correction," *Applied Optics* **44**, pp. 5524–5535, 2005.
2. R. B. Menghua Wang, Bryan A. Franz and C. McClain, "Effects of spectral bandpass on seawifs-retrieved near-surface optical properties of the ocean," *Applied Optics* **40**, pp. 343–347, 2001.

3. Charles R. McClain, Gene C. Feldman, Stanford B. Hooker, "An overview of the SeaWIFS project and strategies for producing a climate research quality global ocean bio-optical time series," *Deep-Sea Res. II* **51**, pp. 5–42, 2004.
4. Mark E. Wilson, Charles McClain, Bryan Monosmith, Manuel Quijada, Eugene Waluschka, Patrick L. Thompsona, Steven Brown, "Optical design of the ocean radiometer for carbon assessment," in *Earth Observing Systems XVI, Proc. SPIE* **8153**, 2011.
5. Eugene Waluschka, Mark Wilson, Manuel Quijada, Brendan McAndrew, Leibo Ding, "Orca depolarizer," in *Polarization Science and Remote Sensing V, Proc. SPIE* **8160**, 2011.
6. Edward Collett, *Field Guide to Polarization*, SPIE Field Guide vol. **FG05**, SPIE Press, Bellingham, Washington, 2005.
7. John G. Hagopian, Stephanie A. Getty, Manuel Quijada, June Tveekrem, Ron Shiri, Patrick Roman, James Butler, Georgi Georgiev, Jeff Livas, Cleophus Hunt, Alejandro Maldonado, "Multiwalled carbon nanotubes for stray light suppression in space flight instruments," *Proc. SPIE* **7761**, p. 77610F, 2010.